A comparative study on stress intensity factor-based criteria for the prediction of mixed mode I-II crack propagation in concrete

Wei Dong[1], Zhimin Wu[2,*], Xuchao Tang[3], Xiangming Zhou[4],

[1]Associate Professor, State Key Laboratory of Coastal and Offshore Engineering, Dalian University of Technology, Dalian 116024, P. R. China. E-mail: dongwei@dlut.edu.cn

[2]Professor, State Key Laboratory of Coastal and Offshore Engineering, Dalian University of Technology, Dalian 116024, P. R. China.

(*Corresponding author). E-mail: wuzhimin@dlut.edu.cn

[3]Postgratuate student, State Key Laboratory of Coastal and Offshore Engineering, Dalian University of Technology, Dalian 116024, P. R. China. E-mail: txc656@163.com

[4]Reader in Civil Engineering Design, Department of Civil and Environmental Engineering, Brunel University London, UB8 3PH, United Kingdom. E-mail: xiangming.zhou@brunel.ac.uk

ABSTRACT

Combined with the fictitious crack model, the stress intensity factor (SIF)-based criteria are widely adopted to determine the crack propagation of mixed mode I-II fracture in normal strength concrete. However, less research is reported on the applicability of the different SIF-based criteria when they are used to analyze the crack propagation process of concrete with different strength grades. With this objective in mind, three-point bending and four-point shear tests were conducted in this study on C20, C50 and C80 grade concrete to measure the initial fracture toughness, fracture energy, load-crack mouth opening/sliding displacement (CMOD/CMSD). Four SIF-based criteria, including two initial fracture toughness-based (with/without mode II component of SIF K_{II}) and two nil SIF-based (with/without K_{II}), were introduced to determine crack propagation and predict the *P-CMOD/CMSD* curves for the notched concrete beams under four-point shear loading. The results indicated that the difference between the peak loads from experiment and from the analysis based on the nil SIF criterion with K_{II} approximately increases with the increase of the concrete strength. By contrast, the predicted peak load and *P-CMOD/CMSD* curves adopting the initial fracture toughness-based criterion with K_{II} showed better agreement with experimental results for the different concrete strength. Meanwhile, in the case of the initial fracture toughness-based criteria, the predicted initial load was underestimated if the component of K_{II} was not considered. However, the fracture mode transformed from mixed mode I-II to mode I after the crack initiation, meaning the K_{II} component in the criterion had a less significant effect on the crack propagation process.

Keywords: Concrete; mixed mode I-II fracture; crack propagation criterion; initial fracture toughness; crack propagation process

1. Introduction

Due to the asymmetries of the structural geometries and the complexities of the loading conditions, cracks in the concrete structures are typically under the bending-shear combined stress field, which the initiation and propagation of the cracks are under the mixed mode I-II fracture. The fracture process of mixed mode I-II in concrete is usually characterized as the formation of micro-cracks that eventually merge and form a propagating macro-crack. The micro-cracks region in concrete is called the fracture process zone (FPZ), which reflects the nonlinear characteristic of concrete as a quasi-brittle material. Its formation is also closely related to the aggregate size because of the high heterogeneity and stress concentration at the notch tip for the concrete structures with big aggregate sizes. According to the fictitious crack model [1], the nonlinear characteristic of the micro-cracks region can be described using the relationship of the crack opening displacement (COD) and cohesive stress acting on the FPZ. However, it should be noted that the stress field at the tip of the crack caused by the applied load will change as the crack propagates under mixed mode I-II fracture. In addition, the COD variation along the FPZ during the fracture process also determines the cohesive stress distribution, which is regarded as the contribution of crack propagation resistance. Both the stress field at the tip of the crack and the cohesive stress distribution along the FPZ affect the crack propagation trajectory under mixed mode I-II fracture. Therefore, for the purpose of the assurance of concrete structures safety and durability, it is significant to develop effective numerical methods to simulate the whole crack propagation process under mixed mode I-II fracture.

In the simulation of a fracture process, an appropriate criterion is a prerequisite for determining crack propagation in concrete. In the case of mixed mode I-II fracture, two main issues should be figured out in the criterion, namely the crack propagation condition and crack propagation angle. Based on the fictitious crack model, there are four types of criteria commonly used in the mixed mode I-II fracture analyses of concrete, including stress-based, strain-based, energy-based and stress intensity factor (SIF)-based. By considering the extremely small size of the plastic zone at the fictitious crack tip, the principle tensile stress and maximum tangential stress criteria have been employed to determine the mixed mode I-II crack propagation in concrete [2-5]. Under the criteria, a crack begins to propagate when the principle tensile stress or maximum tangential stress at the tip of the crack is greater than the uniaxial tensile strength of concrete, and the crack propagates in the direction normal to the tensile stress at the crack tip. According to the maximum tangential stress criteria, a multi-parameter fracture criterion was proposed for concrete to estimate its crack propagation direction under the mixed mode I-II fracture. Meanwhile, some strain-based criteria [6-8] were proposed to determine the crack propagation of the mixed mode I-II fracture of concrete based on the maximum tangential strain criterion. Similar to the maximum tangential stress criterion, the crack propagates in the direction where the tangential strain reaches its maximum value. In the case of the energy-based criterion, Xie et al. [9] proposed an energy approach based on the principle of energy conservation, and predicted the propagation of a quasi-static cohesive crack. In this criterion, a crack propagates when the strain energy release rate exceeds the energy dissipation rate in the FPZ. It should be noted that the crack propagation angle cannot be derived solely from the energy-based theory. In fact, in this criterion, the crack propagation direction is determined by the direction of the principal stress rather than the direction with the maximum energy release rate. Thereafter, the energy-based criterion has been introduced in the simulation of mixed mode I-II crack propagation in concrete [10, 11]. Recently, a new energy-based criterion was proposed for the mixed mode I-II fracture in lightweight aggregate concrete, which can be used to determine the continuous crack propagation along a non-prescribed path and the crack penetration through a material interface[12].

Regarding the SIF-based criteria, the widely adopted approaches were to establish the equilibrium condition of the SIF caused by the applied load K_p and the one caused by the cohesive stress along the FPZ K_σ. However, it should be noted that there were two different viewpoints on the assessment of the difference between K_p and K_σ in the SIF-based criteria. One of them was the nil SIF criterion, which considered the SIF of mode I K_I to vanish at the tip of the FPZ and formulated as $K_p - K_\sigma = K_\mathrm{I} \geq 0$. This criterion was firstly proposed aiming at mode I crack propagation [13], and was introduced in the fracture analyses of fiber-reinforced mortar [14] and concrete [15]. Thereafter, the nil SIF criterion was also extended to fracture analyses of mixed mode I-II in concrete [16-18]. In those studies of mixed mode I-II fracture, the crack propagation angle was determined based on the maximum circumferential stress criterion. In fact, the nil SIF criterion can be regarded as a simplified maximum circumferential stress criterion expressed by the SIFs. The experimental results have verified that local mode I crack growth can be assumed when the crack propagates in a stable manner under loading of mixed mode I-II [19]. Therefore, the simplification of not taking into account K_{II} in crack propagation is reasonable because K_{II} is very small and has less effect in comparison with K_I. However, K_{II} should be considered when determining the crack propagation angle, because it has a significant effect on the crack trajectory even though it is very small. The nil SIF criterion was also used to determine the crack propagation at the rock-concrete interface, although the crack propagation direction was assumed to be along the interface [20].

On the other hand, some researchers claimed that the relationship of the SIFs at the tip of crack represents the competition between the crack driving force attempting to open the crack and the cohesive force attempting to close it. Therefore, the crack resistance properties of concrete should be considered when establishing the equilibrium condition of the SIFs at the tip of crack. Foot et al [21] proposed the critical toughness criterion for cementitious materials, in which the crack can propagate when the difference between the SIF's caused by the driving force and the one by cohesive force exceeds the critical toughness of mortar K_m, i.e. $K_I \geq K_m$. This criterion has been introduced to simulate the mode I crack propagation [22], and calculate the resistance curve of cementitious materials and their fibre-reinforced composites [23]. Recently, by considering concrete as a homogeneous material, an initial fracture toughness criterion [24] was proposed by replacing K_m with the initial fracture toughness of concrete K_{IC}^{ini}. This criterion has been employed to calculate the R-curve[25] and variation of PFZ [26] and predict the peak load [27] of mode I fracture in concrete. Thereafter, aiming at the crack propagation of mixed mode I-II fracture in concrete, Wu et al [28] proposed a new crack propagation criterion by combing the maximum circumferential stress criterion and initial fracture toughness $K_{\mathrm{IC}}^{\mathrm{ini}}$. The crack propagation condition can be written as $K_{(\mathrm{I,II})}^{\mathrm{P}} - K_{(\mathrm{I,II})}^{\sigma} = K_{(\mathrm{I,II})}^{\mathrm{ini}}$, in which $K_{(\mathrm{I,II})}^{\mathrm{P}}$ and $K_{(\mathrm{I,II})}^{\sigma}$ are the combined SIFs of mode I and II caused by the applied load and cohesive forces, respectively. Crack propagates in the direction normal to the principle tensile strain at the tip of the crack. In this criterion, the effect of SIFs of mode II on crack propagation condition was considered. The initial fracture toughness of mode I was introduced as the crack resistance characteristic of concrete, which indicated that the crack propagation condition was still mode I dominated. In addition, an initial fracture toughness criterion was derived through fitting the experimental data to simulate the crack propagation of the rock-concrete interface under mixed mode I-II fracture [29].

For the above-mentioned SIF-based criteria, there are three different viewpoints on the crack propagation condition: (1) whether the crack resistance characteristic of the material was considered; (2) whether the effect of the SIFs of mode II was considered and (3) whether the different crack propagation angles were adopted. Although reasonable agreements have been obtained between the numerical and experimental results for the normal strength concrete using different SIF-based criteria, to the best of the authors' knowledge, no research has been reported on the performance of those different criteria being employed for analyzing fracture of concretes with different strength grades. In particular, the initial fracture toughness $K_{\mathrm{IC}}^{\mathrm{ini}}$ increases with concrete strength, which may lead to significantly different results among the various SIF-based criteria. In addition, it is necessary to elaborate the effect of the SIF of mode II in the crack propagation condition with respect to concrete with different strength grades.

In line with this, the main objective of this paper was to present a comparative study on the simulation of crack propagation under mixed mode I-II fracture using four SIF-based criteria, including nil-SIF and initial fracture toughness criteria with/without K_{II}, respectively. Three-point bending and four-point shear tests were conducted on concrete beams with strength grades C20, C50 and C80 to measure the fracture parameters, and obtain the crack propagation trajectories and load versus crack opening/sliding (P-CMSD/CMSD) curves. The four SIF-based criteria were employed to simulate the crack propagation process of mixed mode I-II. By comparing the numerical and experimental results, the applicability of the four propagation criteria on mixed mode I-II fracture for different strength concrete was evaluated. In addition, the effect of K_{II} in the criteria on crack propagation was discussed. It is expected that this study can provide a valuable assessment on the selection of criteria in analyzing failure behaviors of structures in practical engineering design.

2. Review of four SIF-based criteria

2.1 Criterion I: Initial fracture toughness-based criterion with K_{II}

Combining with the maximum circumferential stress criterion, Wu et al. [28] proposed the crack propagation criterion based on the initial fracture toughness K_{IC}^{ini}. The crack propagation condition can be determined by Eq. (1)

$$\cos\frac{\theta_0}{2}\left[\left(K_I^P - K_I^\sigma\right)\cos^2\frac{\theta_0}{2} - \frac{3}{2}\left(K_{II}^P - K_{II}^\sigma\right)\sin\theta_0\right] = K_{IC}^{ini} \tag{1}$$

Where, K_I^P and K_I^σ are the SIFs of mode I caused by the applied load and cohesive forces, respectively. K_{II}^P and K_{II}^σ are the SIFs of mode II caused by the applied load and cohesive forces, respectively. θ_0 can be defined by Eq. (2).

$$\theta_0 = 2\arctan\frac{\left(K_{\mathrm{I}}^{\mathrm{P}} - K_{\mathrm{I}}^{\sigma}\right) \pm \sqrt{\left(K_{\mathrm{I}}^{\mathrm{P}} - K_{\mathrm{I}}^{\sigma}\right)^2 + 8\left(K_{\mathrm{II}}^{\mathrm{P}} - K_{\mathrm{II}}^{\sigma}\right)^2}}{4\left(K_{\mathrm{II}}^{\mathrm{P}} - K_{\mathrm{II}}^{\sigma}\right)} \quad (2)$$

Substituting Eq. (2) into Eq. (1), the crack propagation condition can be determined. In Criterion I, the crack propagated in the direction normal to the principle strain at the crack tip, of which the propagation angle *α* can be calculated using Eq. (3).

$$\alpha = \frac{1}{2}\arctan\frac{\gamma_{\mathrm{xy}}}{\varepsilon_{\mathrm{x}} - \varepsilon_{\mathrm{y}}} \quad (3)$$

Where, γ_{xy} is the shear strain at the crack tip. ε_{x} and ε_{y} are the normal strains along the X- and Y- axis, respectively.

2.2 Criterion II: Initial fracture toughness-based criterion without K_{II}

Since experimental results [19] have verified that the fracture is mode I dominated in the case of mixed mode I-II, the effect of K_{II} can be neglected in the crack propagation condition. Therefore, Eq. (1) can be written as Eq. (4) by ignoring $K_{\mathrm{II}}^{\mathrm{P}}$ and K_{II}^{σ} in Eqs. (1) and (2), yielding

$$K_{\mathrm{I}}^{\mathrm{P}} - K_{\mathrm{I}}^{\sigma} = K_{\mathrm{IC}}^{\mathrm{ini}} \quad (4)$$

In Criterion II, the crack propagation angle is determined by Eq. (3).

2.3 Criterion III: nil SIF-based criterion with K_{II}

Compared with Criterion I, K_{I} is considered to have vanished at the tip of the FPZ in criterion III. Therefore, the crack resistance characteristic of concrete, i.e. K_{ini}, is replaced by zero. Meanwhile, the effects of $K_{\mathrm{II}}^{\mathrm{P}}$ and K_{II}^{σ} are considered in this criterion. Then, the crack propagation condition can be written as Eq. (5).

$$\cos\frac{\theta_0}{2}\left[\left(K_{\mathrm{I}}^{\mathrm{P}} - K_{\mathrm{I}}^{\sigma}\right)\cos^2\frac{\theta_0}{2} - \frac{3}{2}\left(K_{\mathrm{II}}^{\mathrm{P}} - K_{\mathrm{II}}^{\sigma}\right)\sin\theta_0\right] = 0 \quad (5)$$

Accordingly, the crack propagation angle is determined by Eq. (3).

2.4 Criterion IV: nil SIF-based criterion without K_{II}

Compared with Criterion III, the effect of $K_{\mathrm{II}}^{\mathrm{P}}$ and K_{II}^{σ} on the crack propagation condition is not considered in this criterion. Therefore, the crack propagation condition can be written as Eq. (6).

$$K_{\mathrm{I}}^{\mathrm{P}} - K_{\mathrm{I}}^{\sigma} = 0 \tag{6}$$

Accordingly, the crack propagation angle is determined by Eq. (3).

In summary, the expressions of the four SIF-based criteria are listed in Table 1. It should be noted that to clarify the effect of the propagation condition on the fracture process, the same equation of the crack propagation angle is adopted for the different criteria.

Table 1. Expressions of various SIF-based criteria

Criterion	Propagation condition	Propagation angle
I	$\cos\frac{\theta_0}{2}\left[\left(K_{\mathrm{I}}^{\mathrm{P}} - K_{\mathrm{I}}^{\sigma}\right)\cos^2\frac{\theta_0}{2} - \frac{3}{2}\left(K_{\mathrm{II}}^{\mathrm{P}} - K_{\mathrm{II}}^{\sigma}\right)\sin\theta_0\right] = K_{\mathrm{IC}}^{\mathrm{ini}}$	
II	$K_{\mathrm{I}}^{\mathrm{P}} - K_{\mathrm{I}}^{\sigma} = K_{\mathrm{IC}}^{\mathrm{ini}}$	$\alpha = \frac{1}{2}\arctan\frac{\gamma_{\mathrm{xy}}}{\varepsilon_{\mathrm{x}} - \varepsilon_{\mathrm{y}}}$
III	$\cos\frac{\theta_0}{2}\left[\left(K_{\mathrm{I}}^{\mathrm{P}} - K_{\mathrm{I}}^{\sigma}\right)\cos^2\frac{\theta_0}{2} - \frac{3}{2}\left(K_{\mathrm{II}}^{\mathrm{P}} - K_{\mathrm{II}}^{\sigma}\right)\sin\theta_0\right] = 0$	
IV	$K_{\mathrm{I}}^{\mathrm{P}} - K_{\mathrm{I}}^{\sigma} = 0$	

3. Numerical simulation

In this study, ANSYS finite element code was used to conduct the simulation of crack propagation under mixed mode I-II fracture. Singular element was adopted to calculate SIF at the crack tip by means of the displacement extrapolation method. Due to the quasi-brittle characteristics of concrete, there exist cohesive forces along the FPZ, which contribute to the crack resistance during the crack propagation. In this study, a bilinear softening relationship between the cohesive stress (σ) versus the crack opening displacement (w) was employed in the numerical analysis which can be formulated as follows:

$$\sigma = f_t - (f_t - \sigma_s)\frac{w}{w_s} \qquad \text{for } 0 \le w \le w_s \qquad (7)$$

$$\sigma = \sigma_s \frac{w_0 - w}{w_0 - w_s} \qquad \text{for } w_s < w \le w_0 \qquad (8)$$

$$\sigma = 0 \qquad \text{for } w > w_0 \qquad (9)$$

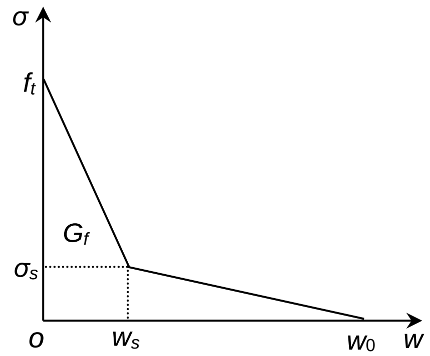

Fig. 1. Bilinear σ-w concrete softening curve

According to Petersson [30], σ_s, w_s and w_0 can be determined as follows:

$$\sigma_s = f_t/3 \qquad (10)$$

$$w_s = 0.8G_f/f_t \qquad (11)$$

$$w_0 = 3.6G_f/f_t \qquad (12)$$

where G_f is the fracture energy and f_t is the uniaxial tensile strength of concrete. w_s and σ_s are the crack opening displacement and the corresponding cohesive stress respectively at the break-point of the bilinear σ-w relationship. w_0 is the stress-free crack opening displacement (see Fig. 1). It should be noted that, in the case of mixed mode I-II fracture, the crack opening displacement w is the vector sum of a normal component, w_1, and a tangential component, w_2, i.e. $w=\sqrt{w_1^2+w_2^2}$. In this study, it was assumed that w affects the energy dissipation and is associated with the cohesive stresses. Consequently, the end of the FPZ was determined by a comparison of w with w_0.

The four SIF-based crack propagation criteria were then introduced into the numerical simulation of the crack propagation process of mixed mode I-II. In this study, singular element was employed to calculate the SIF at the tip of crack. A circle was set at the tip of crack, in which the crack tip is the center of the circle and the crack propagation incremental length Δa=2 mm is the radius of the circle. The first row of elements around the crack tip had a radius of $\Delta a/6$, and the mid-side nodes were placed at the quarter points, i.e. located on the circle with a radius of $\Delta a/24$. The program flow diagram of the iterative numerical process is illustrated in Fig. 2, and the numerical procedure is shown in the following steps:

1. Input data, $P(1) = P_{ini}$, $a(1) = a_0$. Calculate $\alpha(1)$ based on P_{ini} from experiment.
2. Establish the numerical model for four-point shear (FPS) beam with crack length $a_{i,j} = a(j\text{-}1) + \Delta a$ (i = 1,2…, j = 2,3…) and crack propagation angle $\alpha(\text{j-1})$. In the case of j>2, delete the mesh mode and re-mesh the mode according to the information from the saved j-1 step. Here Δa is a specified increment of crack length chosen in numerical analysis, where *i* represents the load increment during the iteration process with a same crack length and *j* represents the crack length increment during the iteration analyses.
3. Apply load $P_{i,j}$ to the FPS beam and calculate cohesive stress $\sigma_{i,j}$ using Eqs. (7)-(9). Calculate SIFs (K_{I}^{P}, K_{I}^{σ}, K_{II}^{P} and K_{II}^{σ} for Criterion I and III, and K_{I}^{P} *and* K_{I}^{σ} for Criteria II and IV) by adjusting load $P_{i,j}$ until the crack propagation condition in the relevant criterion is satisfied. Calculate $\alpha(\text{j})$ using Eq. (3) and derive CMOD(j) and CMSD(j) based on the numerical results.

4. Save the calculated results of $P_{i,j}$, $a_{i,j}$, CMOD(j) and CMSD(j).

5. Repeat steps 2-4 for the next crack propagation. The iterative process terminates when the crack tip is close to the boundary of the specimen or the value of the applied load becomes negative.

Therefore, upon obtaining K_{ini}, G_f, f_t and elastic modulus, E, of concrete from experiment, the whole fracture process, including *P-CMOD and P-CMSD* curves, can be obtained by repeating the above exercise. Details of the iterative numerical process for predicting crack propagation using Criterion I can be found in Reference[28]. Taking Specimen FPS-50-40 as an example, Fig. 3 illustrates the deformation of various crack propagation stages, including crack initiation, unstable propagation and failure. The size and loading condition of Specimen FPS-50-40 are listed in Table 3.

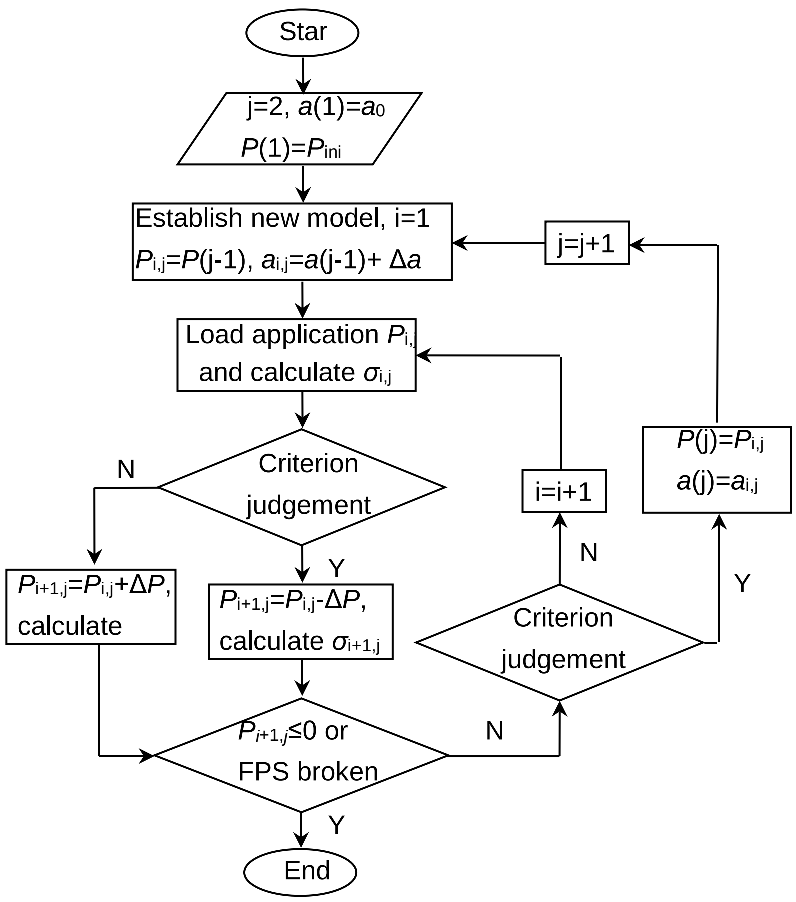

Fig. 2. Program flow diagram for the numerical simulation

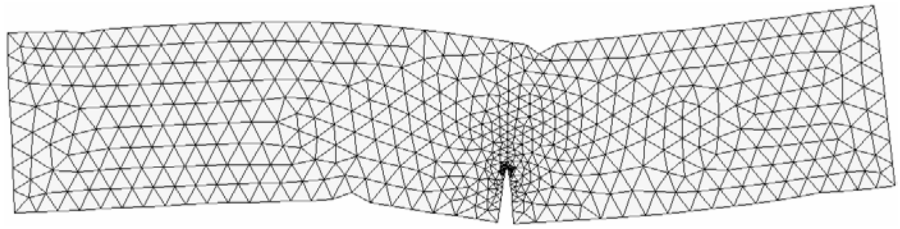

(a) Crack initiation

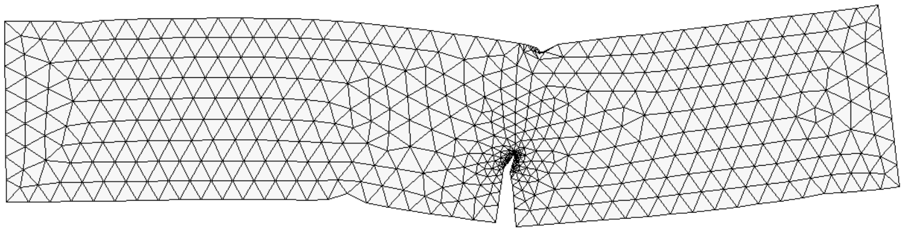

(b) Crack unstable propagation

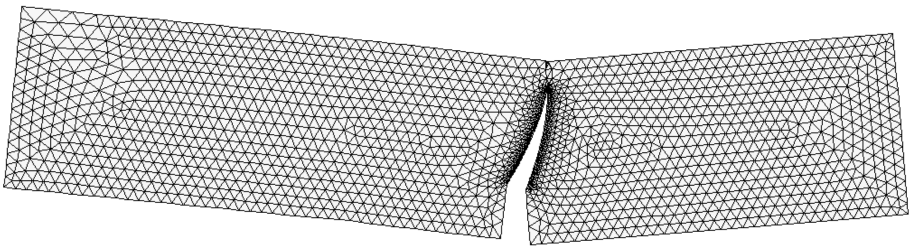

(c) Failure

Fig. 3. Deformation of various crack propagation stages for Specimen FPS-50-40

4. Experimental program

To verify the four SIF-based criteria, three series of three-point bending (TPB) and four-point shear (FPS) beams, with concrete strength grades C20, C50 and C80, were tested to investigate the crack propagation process. Four specimens were prepared for the same geometry and loading condition. Mix proportions of the concrete with different strength grades are listed in Table 2. Crushed limestone with a maximum size of 20 mm was used as coarse aggregate and medium-size river sand was used as fine aggregate. The C20 and C50, and C80 concretes were made with Grade R42.5 and R52.5 Portland cements, respectively (Chinese standard of Common Portland Cement, GB175-2007). To improve the workability of the C80 concrete which had a lower water-to-cement ratio, a water reducing admixture was added.

Table 2. Mix proportions of concretes targetting different strength grades

Concrete	Cement grade	Cement	Sand	Aggregate	Water	Fly ash	Water reducing admixture
		(kg/m^3)					
C20	R42.5	216	715	1167	210	92	-
C50	R42.5	446	595	1105	214	-	-
C80	R52.5	390	632	1225	142	61	6.31

The beams in each series had the same dimension, i.e., Length (L)×Height (H)×Breadth (B)=580 mm×120 mm× 60 mm and the initial crack length/depth ratio a_0/D was equal to 0.3. To obtain the different combinations of K_{I} and K_{II} at the pre-crack tip, the positions of the pre-crack and loading points were adjusted in each series of FPS beams. The geometry and loading arrangement of the beams are illustrated in Fig. 4. Here, a_0 is the pre-crack length; C, L_1 and C_1 are the distances from the two loading points and pre-notch to the geometric center of the specimens, respectively.

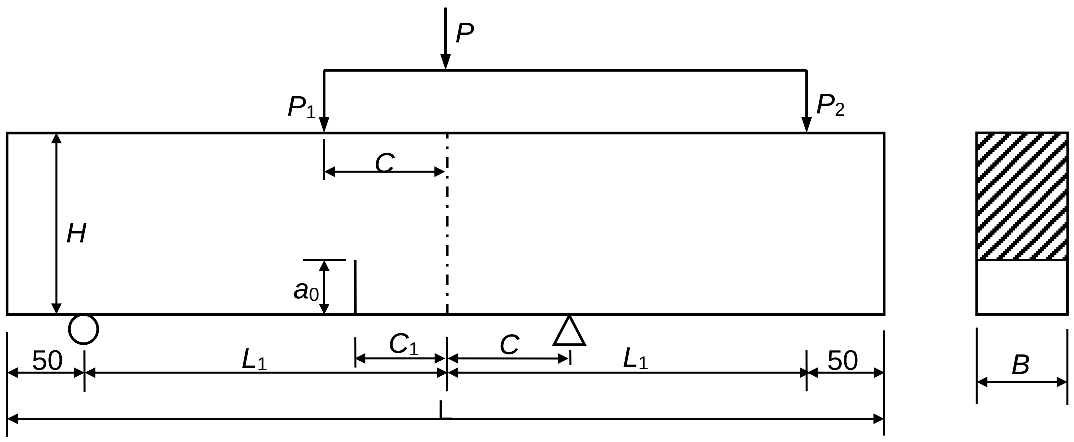

Fig. 4. Specimen geometry and experimental set-up under FPS

The sizes and loading conditions of all specimens are listed in Table 3, in which $K_{\mathrm{I}}^{\mathrm{ini}}/K_{\mathrm{II}}^{\mathrm{ini}}$ varies from 0 to infinity, i.e. pure mode I fracture. Here, $K_{\mathrm{I}}^{\mathrm{ini}}$ and $K_{\mathrm{II}}^{\mathrm{ini}}$ are the SIFs of mode I and II corresponding to the crack initiation, respectively. Through changing the position of the pre-crack, i.e. the C_1 value, various combinations of tension and shear at the pre-crack tip can be obtained. With the increase of C_1 value, the tensile stress increases and the shear stress remains the same so that a larger ratio of $K_{\mathrm{I}}/K_{\mathrm{II}}$ can be obtained (see Table 3). Consequently, the increase of C_1 value will also decrease the initial and peak loads due to the variation of the stress distribution at the tip of crack.

The specimen number "TPB-20" denotes a series of TPB beams of C20 strength grade. The specimen number "FPS-20-40" denotes a series of FPS beams of C20 strength grade and C_1=40 mm. Fig. 5 (a) and (b) show the experimental setups for TPB and FPS tests, respectively. The TPB and FPS tests were performed on a 250 kN closed-loop servo-controlled testing machine with stroke displacement rate of 0.036 mm/min.

Table 3. Geometries of TPB and FPS specimens

Nos of specimens	$L\times H\times B$ (mm^3)	a_0 (mm)	C (mm)	C_1 (mm)	L_1 (mm)	$K_{\mathrm{I}}^{\mathrm{ini}}/K_{\mathrm{II}}^{\mathrm{ini}}$
TPB-20			240	0		∞
FPS-20-0			40	0		0
FPS-20-20	580×120×60	36	40	20	240	1.61
FPS-20-40			60	40		3.49
FPS-20-60			80	60		5.32
TPB-50			240	0		∞
FPS-50-0			40	0		0
FPS-50-20	580×120×60	36	40	20	240	1.61
FPS-50-40			60	40		3.49
FPS-50-60			80	60		5.32
TPB-80	580×120×60	36	240	0	240	∞

FPS-80-0	40	0	0
FPS-80-20	40	20	1.61
FPS-80-40	60	40	3.49
FPS-80-60	80	60	5.32

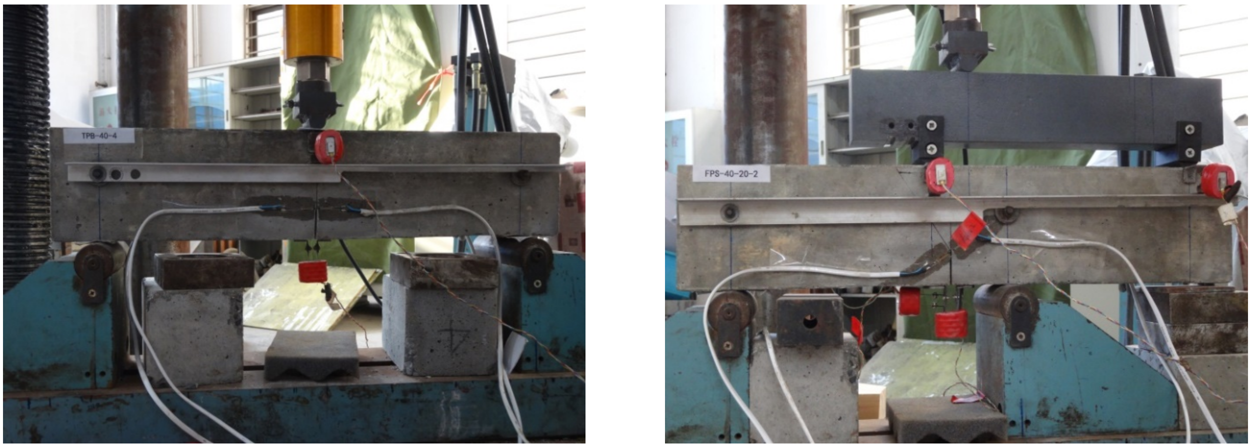

(a) TPB test (b) FPS test

Fig. 5. Experimental set-up of (a) TPB test and (b) FPS test

Mechanical properties of the concrete, including uniaxial compressive strength f_c, uniaxial tensile strength f_t, elastic modulus E were measured from relevant tests. In addition, the fracture parameters, including initial fracture toughness $K_{\mathrm{IC}}^{\mathrm{ini}}$, fracture energy G_f were derived from the TPB tests. G_{f} in Table 4 denotes the fracture energy of mode I and the one of mode II was not considered in this study. Although, the crack tip is under the combination of tension and shear stresses for the mixed mode I-II fracture, the crack initiation and propagation are caused by the principle tension stress due to the low tensile strength of concrete. Therefore, in this paper, only the tension softening constitutive law, i.e. the relationship of σ-w was adopted to characterize the nonlinearity in FPZ.

$K_{\mathrm{IC}}^{\mathrm{ini}}$ can be calculated using Eq. (13) as per reference [31].

$$K_{\mathrm{IC}}^{\mathrm{ini}} = \frac{3P_{\mathrm{ini}}S\sqrt{a_0}}{2H^2B}F_1(a_0 / D) \tag{13}$$

Where, S is the span of the TPB beam and $F_1(a_0/D)$ can be defined by Eq.(14).

$$F_1(a_0/D) = \frac{1.99-(a_0/D)(1-a_0/D)[2.15-3.93(a_0/D)+2.7(a_0/D)^2]}{(1+2a_0/D)(1-a_0/D)^{3/2}} \tag{14}$$

According to Eq. (13), $K_{\mathrm{IC}}^{\mathrm{ini}}$ can be calculated if the initial cracking load P_{ini} and specimen geometry are given. P_{ini} can be determined through the strain variation of the strain gauges, which were attached vertically in front of the pre-crack (see Fig. 5(a)). Once a new crack begins to initiate, the measured strain will decrease from its maximum value due to the release of the fracture energy. Thus, P_{ini} can be determined based on the strain variation around the tip of the pre-crack. The mechanical parameters of the concrete are listed in Table 4.

Table 4. Mechanical properties of the concrete

Concrete	f_c(MPa)	f_t (MPa)	E (GPa)	$K_{\mathrm{IC}}^{\mathrm{ini}}$ (MPa·m$^{1/2}$)	G_f (N/m)
C20	28.90	2.56	25.26	0.49	104.87
C50	59.68	3.93	35.92	0.68	139.57
C80	83.90	4.25	39.48	0.73	147.97

5. Results and discussion

Effect of $K_{\mathrm{IC}}^{\mathrm{ini}}$ on crack propagation

The difference between Criteria I and III is whether $K_{\mathrm{IC}}^{\mathrm{ini}}$ is introduced as the crack resistance in the determination of crack propagation. Therefore, in this section, the *P-CMS*D and *P-CMOD* curves with different concrete strength grades from FPS tests and numerically simulated using Criteria I and III are compared which is illustrated in Fig. 6.

It can be seen from Fig. 6 that the predicted *P-CMOD* and *P-CMSD* curves using Criteria I and III are almost around the envelopes of the experimental results. However, the predicted

$P_{\max}$ using Criterion I are obviously higher than the ones using Criterion III. The peak loads from experiment and prediction using Criterion I and III, and the corresponding errors are listed in Table 5. It should be noted that the average errors are adopted in this table. Accordingly, a comparison is made between the predicted $P_{\max}$ using Criteria I and II and the experimental ones as shown in Fig. 7, in which $P_{\max,\text{pre}}$ and $P_{\max,\text{exp}}$ denote the predicted and experimental peak loads, respectively. It can be seen that, the predicted $P_{\max}$ values using Criterion I are much closer to the experimental results than those using Criterion III. Compared with the experimental results, the predicted $P_{\max}$ using Criterion III are slightly underestimated. This can be explained by analyzing the fracture mechanism based on Criteria I and III. For Criterion I, the crack propagation resistance is considered as a combination of the cohesive force effect along the FPZ and the anti-crack property from concrete, which are expressed by SIFs as $K_{(\text{I,II})}^{\sigma}$ and $K_{\text{IC}}^{\text{ini}}$, respectively. In contrast, in the case of Criterion III, the crack propagation resistance is only provided by the cohesive force action on the FPZ, i.e. $K_{(\text{I,II})}^{\sigma}$. Therefore, compared with Criterion III, the larger applied load is needed for Criterion I to drive the crack propagating from the stable crack stage to the unstable propagation stage.

Meanwhile, $K_{\text{IC}}^{\text{ini}}$ is usually regarded as the inherent property of concrete and its value increases with the increase of concrete strength. In the case of a perfectly plastic material, the deformation resistance is provided by the cohesion of the plastic material so that $K_{\text{IC}}^{\text{ini}}$ can be considered as zero. In this condition, Criteria I and III have the same expression, i.e. $K_{(\text{I,II})}^{\text{p}} - K_{(\text{I,II})}^{\sigma} = 0$. It should be noted that the concept of SIF from the linear elastic fracture model is not applicable for the crack propagation analysis in a plastic material. Here, the plastic condition is employed as a special example to discuss the transformation between Criteria I and III. On the contrary, in the case of a perfectly brittle material, a FPZ and cohesive force do not exist, i.e. $K^{\sigma}_{(\mathrm{I,II})}$=0. In this condition, Criterion I transforms into the maximum circumferential stress criterion expressed by SIFs if $K^{\mathrm{ini}}_{\mathrm{IC}}$ is replaced by $K^{\mathrm{un}}_{\mathrm{IC}}$ ($K^{\mathrm{ini}}_{\mathrm{IC}}$ and $K^{\mathrm{un}}_{\mathrm{IC}}$ are the same for a brittle material). However, at that moment, Criterion III transforms into $K^{\mathrm{p}}_{(\mathrm{I,II})} = 0$. Obviously, it is not a reasonable determination for an unstable crack condition since a structure can fail under even a very small load.

In the case of a quasi-brittle material, e.g. concrete, the nonlinear characteristic is caused by the micro-crack propagation and the effect of the cohesive force acting on the FPZ. With the increase of concrete strength, the brittleness of concrete increases and the initial fracture toughness of concrete $K^{\mathrm{ini}}_{\mathrm{IC}}$ is also enhanced. For Criterion I, the driving force caused by the applied load is balanced with the resistance caused by the cohesive force and $K^{\mathrm{ini}}_{\mathrm{IC}}$. However, for Criterion III, the resistance is only provided by the cohesive force. Therefore, compared with Criterion I, a longer FPZ length is needed for Criterion III to establish the equilibrium between the driving force and resistance at the peak load. Taking the *P-CMOD* curves of FPS-20-60 Series as examples, the critical crack propagation lengths a_c derived from the numerical results using Criteria I and III are 14 mm and 38 mm, respectively. In addition, with the increase of the concrete strength grade from C20, C50 to C80 for FPS-20/50/80-60 Series specimens, the predicted values of a_c based on Criterion III are 38 mm, 36 mm and 34 mm, respectively, which reflect the effect of the enhanced concrete brittleness on the FPZ evolution. On the contrary, the predicted values of a_c based on Criterion I remain as 14 mm for the three concrete grades, and $K^{\mathrm{ini}}_{\mathrm{IC}}$ increases from 0.49

MPa·m$^{1/2}$ to 0.68 MPa·m$^{1/2}$, and then to 0.73 MPa·m$^{1/2}$. This indicates that, for Criterion I, the increase of the concrete strength is reflected by the enhancement of the initial fracture toughness and has less influence on the critical crack propagation length. It should be noted that, the variation of fracture toughness based on LEFM in the case of ductile metal pipes were investigated by Li. et al [32].

Due to the short critical crack propagation length in Criterion I, the value of K_{IC}^{ini} has an increasingly significant effect on crack propagation resistance at the peak load point with the increase of concrete strength. By contrast, since the effect of the initial fracture toughness on crack propagation is not considered in Criterion III, the difference of P_{max} between the predicted and experimental values could increase with the increase of concrete strength. According to the P_{max} obtained from the experiment and from the predicted ones using Criterion III (see Table 5), the average errors for the concrete specimens with C20, C50 and C80 strength grades are 14.12%, 10.30% and 12.10%, respectively. It should be noted that, for FPS-20-0 series specimens, the errors for Criteria I and III are obviously larger than the other specimens with C20 strength grade. This may be caused by the scattered experimental results since only two specimens were tested for the FPS-20-0 series due to the other specimens breaking during demolding. If the FPS-20-0 series specimens are not counted, the average errors of P_{max} for the concrete specimens with C20, C50 and C80 strength grades will be 8.61%, 10.30% and 12.10%, respectively, when Criterion III is adopted. The results show an increase of the errors with the increase of the concrete strength. Accordingly, in the case of Criterion I, the average errors of P_{max} for the specimens with concrete strength grades of C20, C50 and C80 are 3.65%, 5.61% and 5.67%, respectively, which show a much closer agreement compared with the results using Criterion III. Meanwhile, due to the longer critical crack propagation length, the predicted crack mouth opening/sliding displacements $CMOD_c/CMSD_c$ using Criterion III are larger than the ones using Criterion I (See Fig. 6). In summary, compared with Criterion III, the predicted *P-CMOD* and *P-CMSD* curves using Criterion I exhibit a better agreement with the experimental results.

It should be noted that the homogeneity assumption was employed for concrete in this study, i.e. the effect of the maximum aggregate size on the FPZ evolution and crack propagation was not considered. Conventionally, concrete can be approximately regarded as a homogeneous material if the size of a concrete specimen is larger than three times of its maximum aggregate size [33]. However, according to the recent studies [34-37], the maximum aggregate size has significant influence on the fracture properties, including fracture energy, fracture toughness and crack propagation length, of concrete. Furthermore, the influence is also reflected by the values of Pini and Pmax from experiment because the micro-crack formation and fictitious crack propagation is associated with the ratio of maximum aggregate size to the ligament length [38]. Therefore, the influence of aggregates needs to be carefully considered in modeling of quasi-brittle fracture of concrete, so that a better understanding on concrete fracture and the associated size effect [39] can be achieved. Recently, through establishing the relationship between the maximum aggregate size d_{max} and the critical crack propagation length Δa_c, the effects of heterogeneous concrete material structures on quasi-brittle fracture has been validated in terms of the size ratios, a_0/d_{max}, $(H-a_0)/d_{max}$ and $\Delta a_c/d_{max}$ [38, 40-42]. Regarding the experimental results in

Fig.6, there exist large differences between experimental and numerical results in some cases, e.g. FPS-20-60 series specimens, which can be attributed to heterogeneity of concrete. Therefore, further study on the applicability of different criteria with the consideration of effect of maximum aggregate size should be carried out.

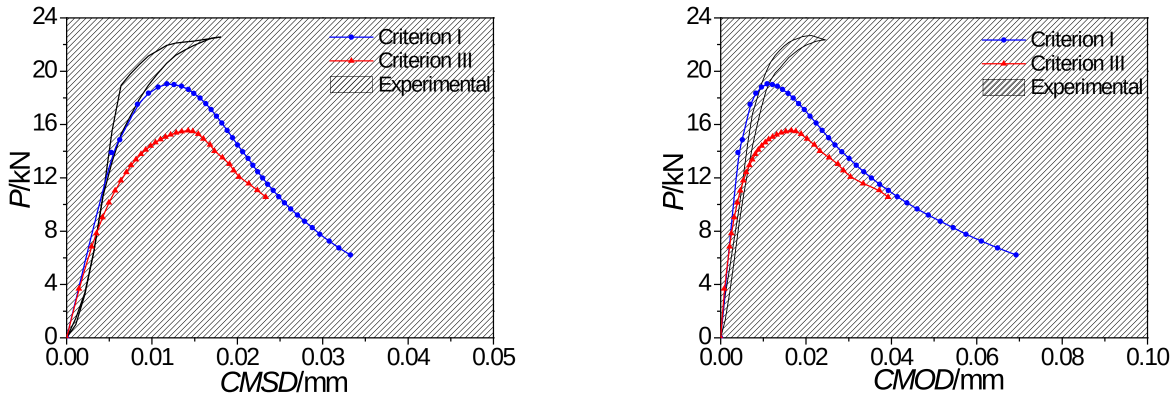

(a) FPS-20-0 Series

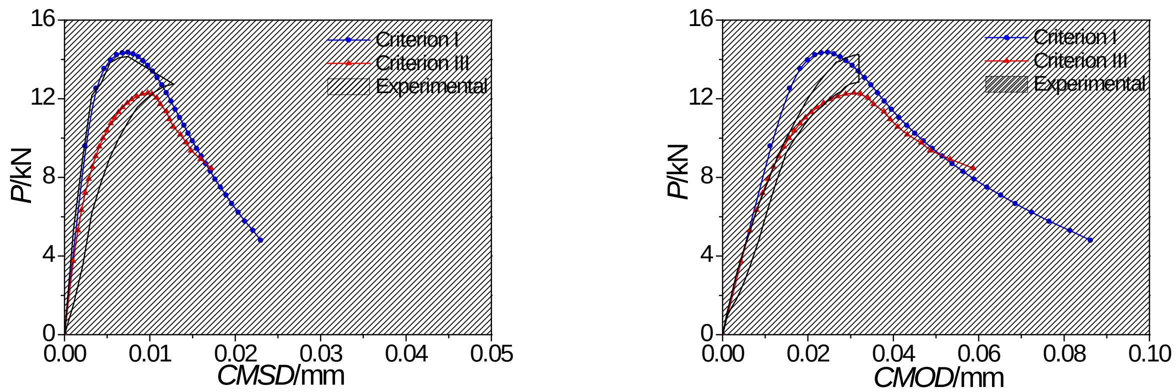

(b) FPS-20-20 Series

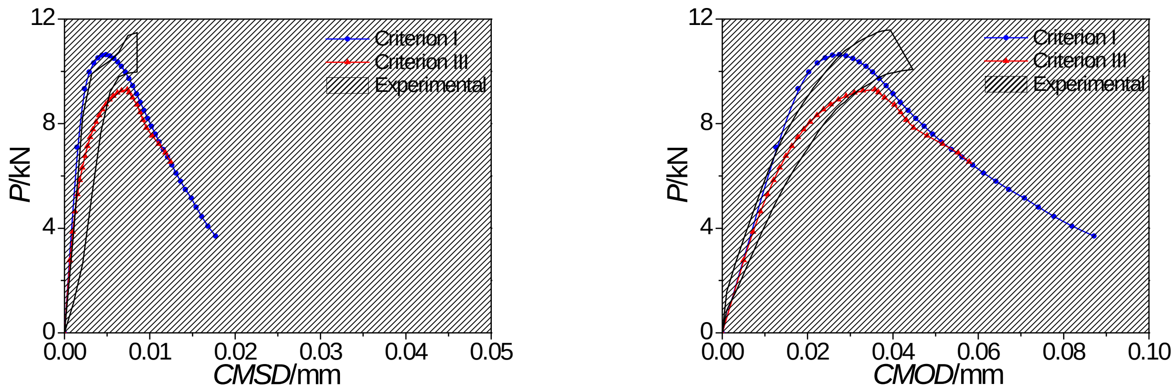

(c) FPS-20-40 Series

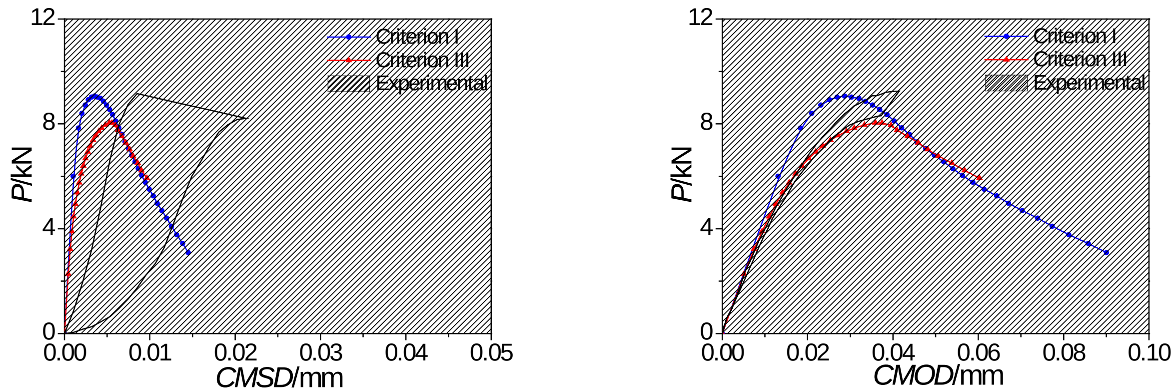

(d) FPS-20-60 Series

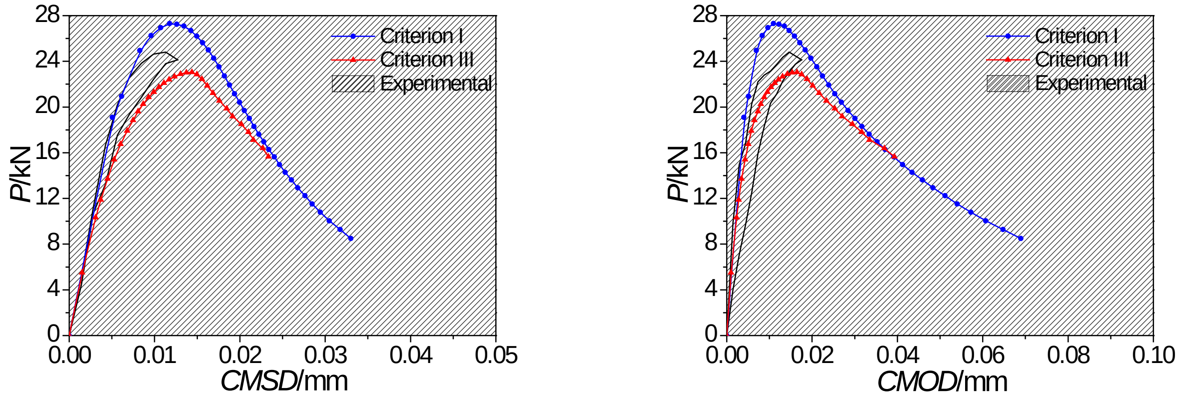

(e) FPS-50-0 Series

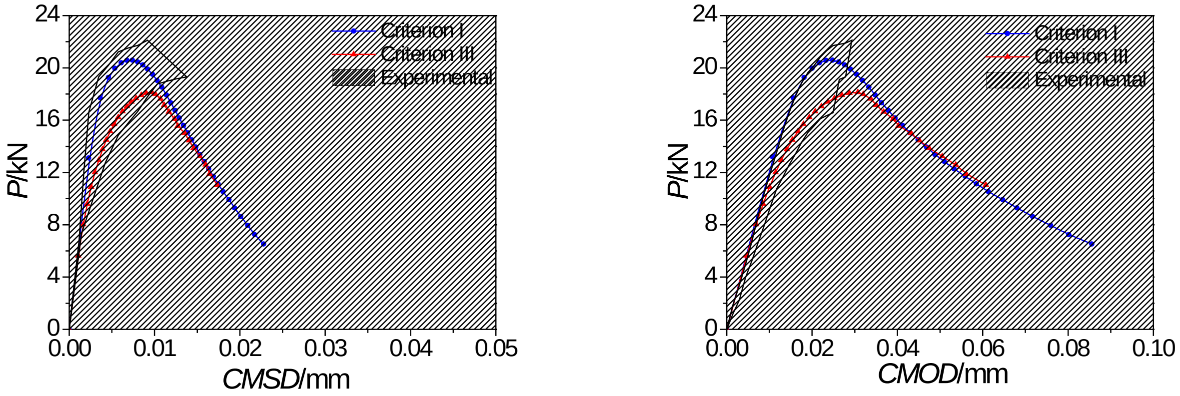

(f) FPS-50-20 Series

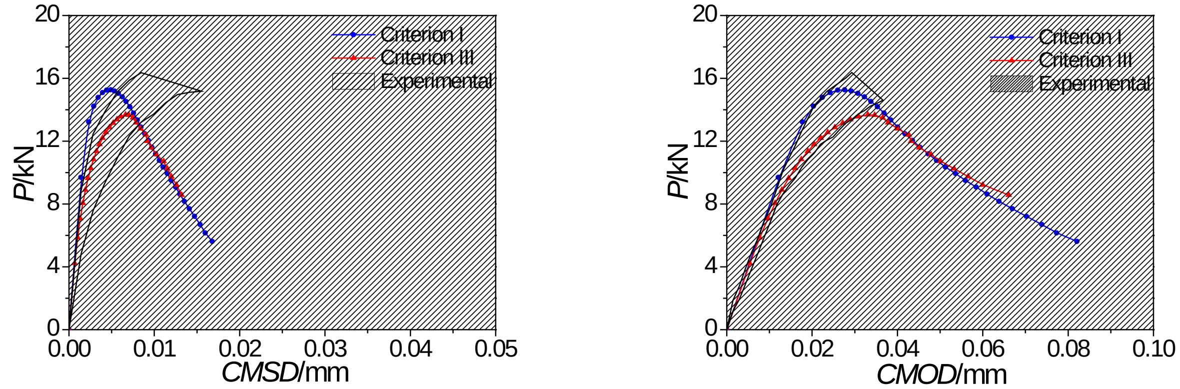

(g) FPS-50-40 Series

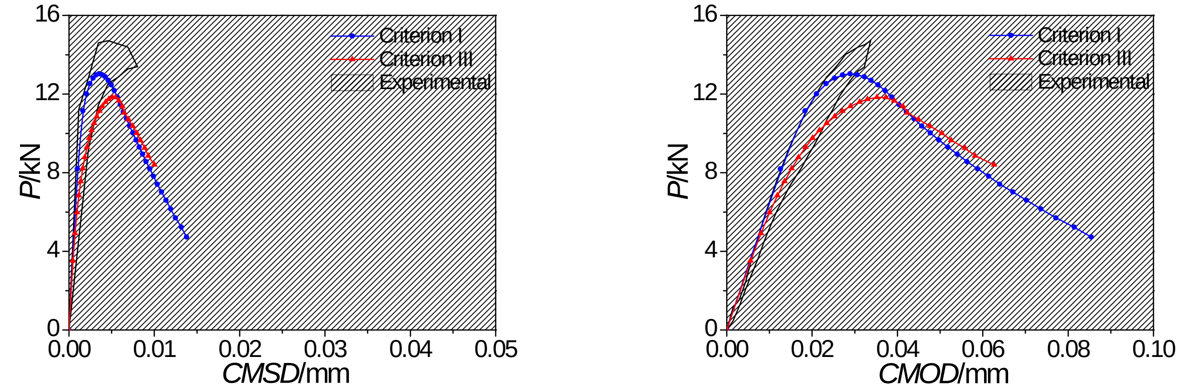

(h) FPS-50-60 Series

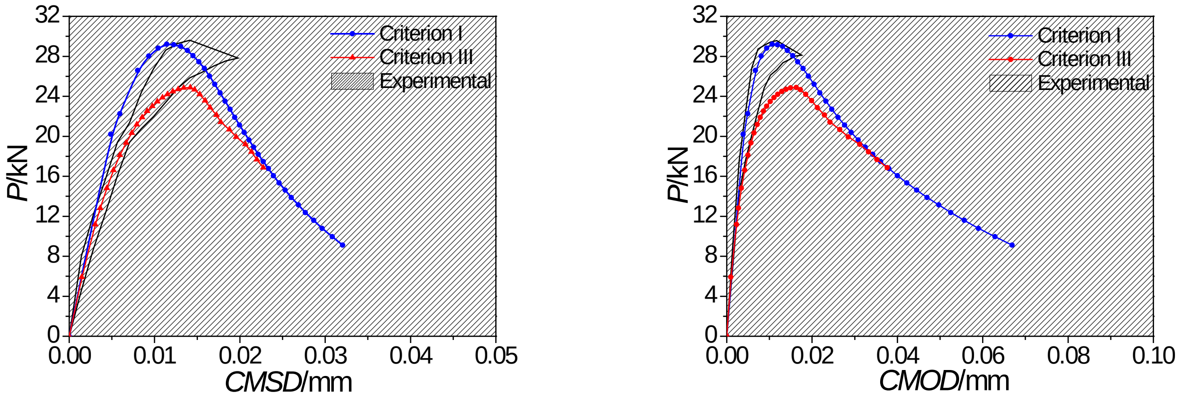

(i) FPS-80-0 Series

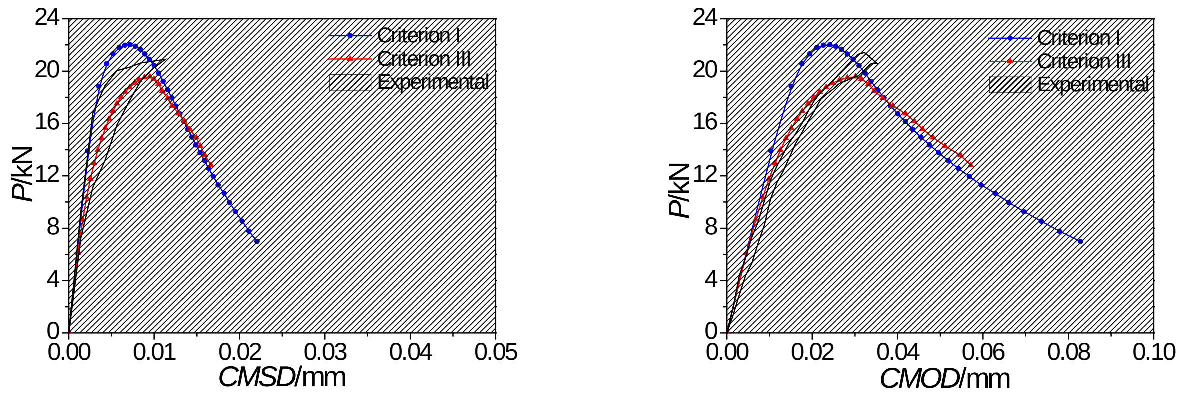

(j) FPS-80-20 Series

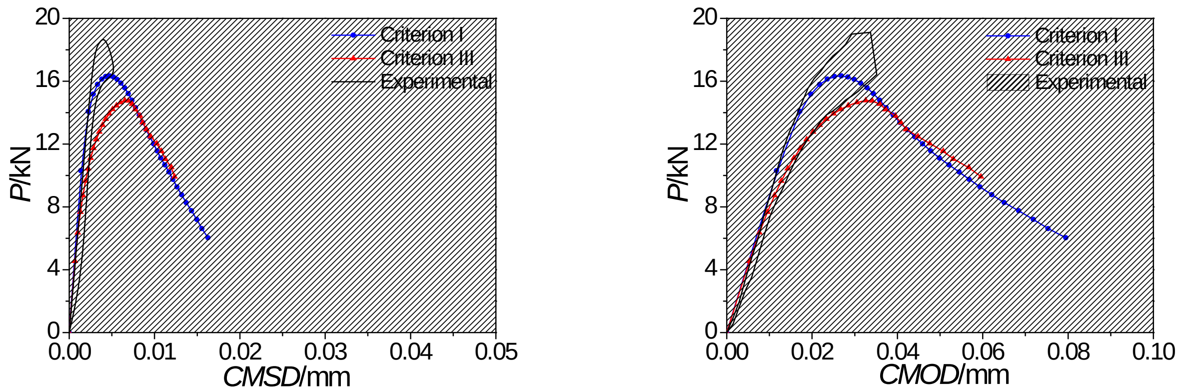

(k) FPS-80-40 Series

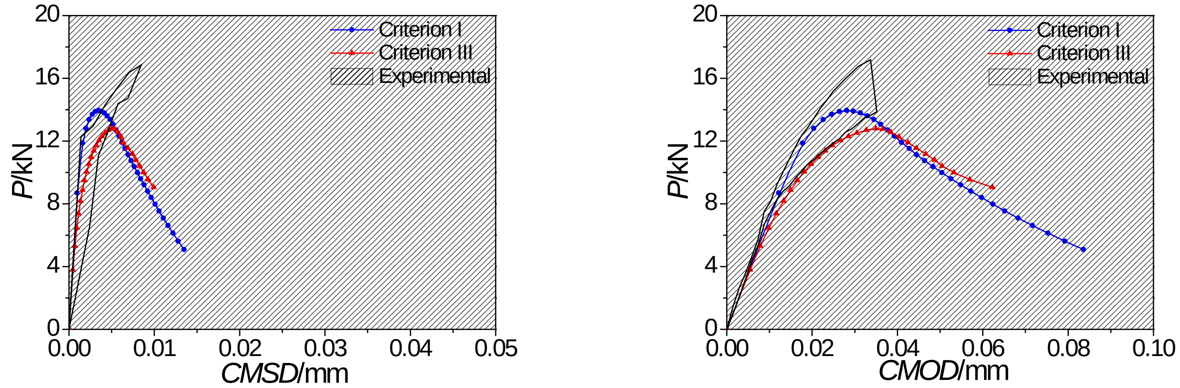

(l) FPS-80-60 Series

Fig. 6. P-*CMSD* and -*CMOD* curves from experiment and numerical simulation using Criteria I and III

Table 5. Comparison of P_{max} from experiment and numerical simulation using Criteria I and III

Nos of specimens	Experimental (kN)	Predicted by using criterion I (kN)	Error (%)	Predicted using criterion III (kN)	Error (%)
FPS-20-0	22.41	19.05	-14.99	15.54	-30.66
FPS-20-20	13.57	14.36	5.82	12.25	-9.73
FPS-20-40	10.56	10.64	0.76	9.30	-8.72
FPS-20-60	8.68	9.06	4.38	8.04	-7.37
FPS-50-0	24.47	27.31	11.61	23.04	-5.84
FPS-50-20	19.93	20.59	3.31	18.14	-8.98
FPS-50-40	15.39	15.27	0.78	13.68	-11.11
FPS-50-60	13.97	13.03	-6.73	11.84	-15.25
FPS-80-0	28.53	29.21	2.38	24.88	-12.79
FPS-80-20	20.66	22.02	6.58	19.58	-5.23
FPS-80-40	17.23	16.34	-5.17	14.78	-14.22
FPS-80-60	15.26	13.95	-8.58	12.80	-16.12

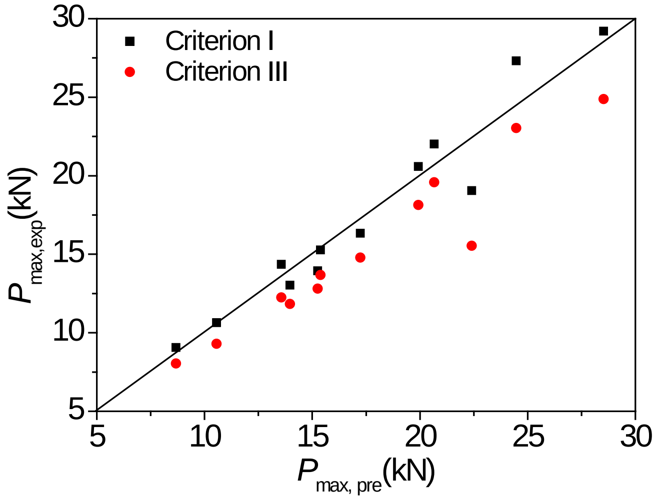

Fig. 7. P_{max} obtained from experiment and numerical simulation

Fig. 8 illustrates the comparison of crack propagation trajectories between the tests and the predictions using Criteria I and III. Although the different crack propagation conditions are adopted in Criteria I and III, the predicted trajectories are almost identical to each other and have strong agreement with the experimental results. It indicates that with or without the introduction of $K_{\mathrm{IC}}^{\mathrm{ini}}$, the crack propagation condition of Criteria I and III does not influence the predicted crack propagation trajectories.

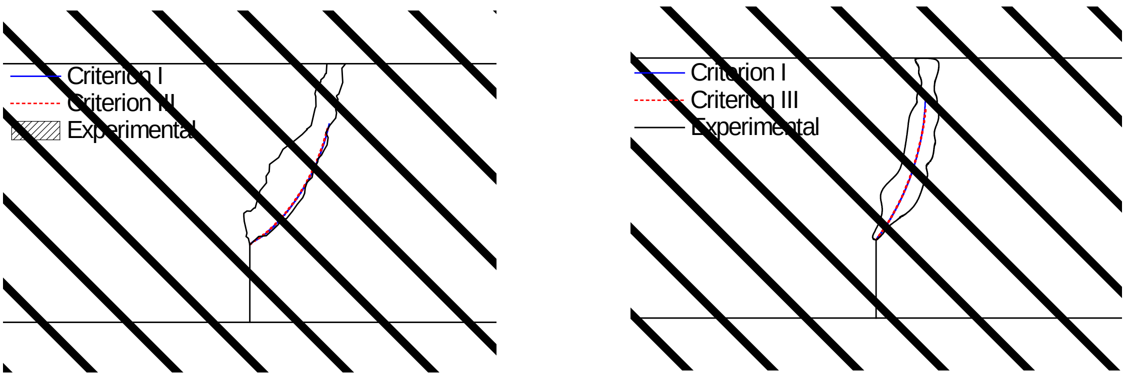

(a) FPS-20-0 Series (b) FPS-20-20 Series

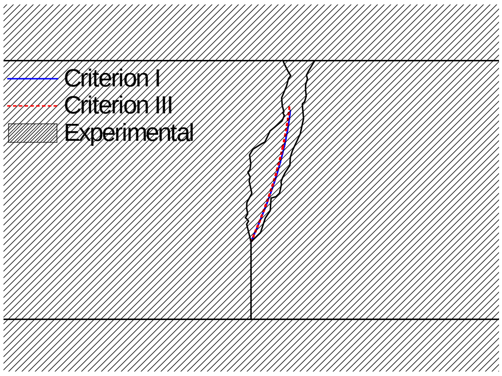

(c) FPS-20-40 Series

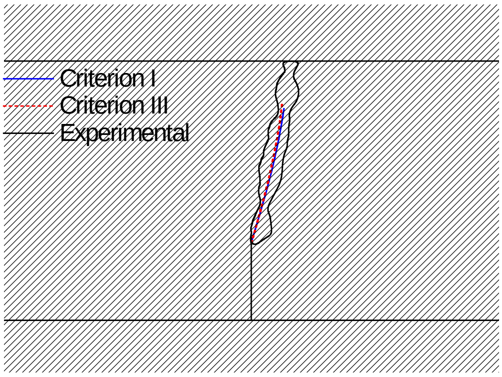

(d) FPS-20-60 Series

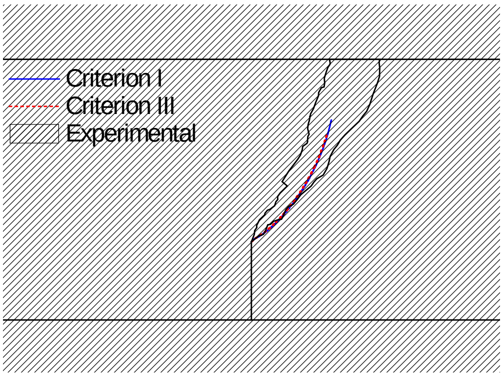

(e) FPS-50-0 Series

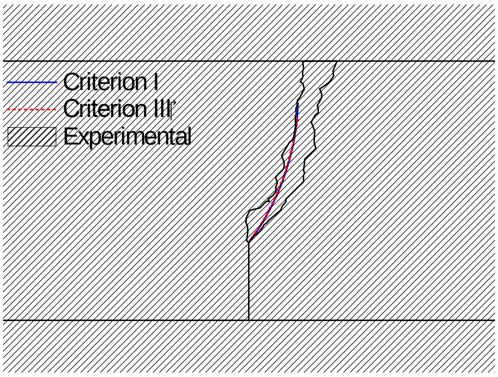

(f) FPS-50-20 Series

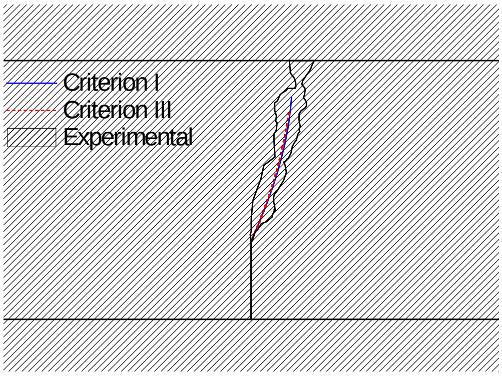

(g) FPS-50-40 Series

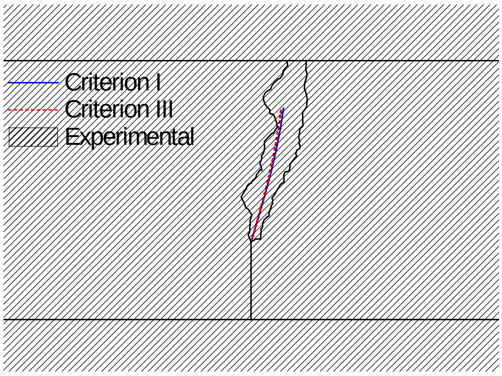

(h) FPS-50-60 Series

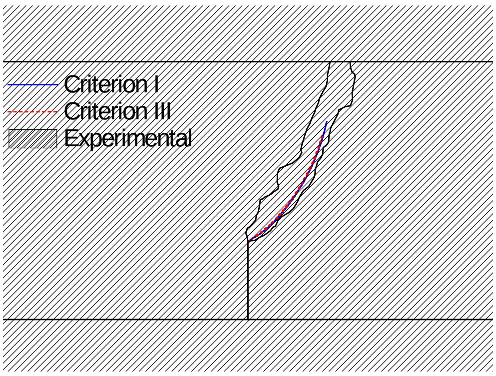

(i) FPS-80-0 Series

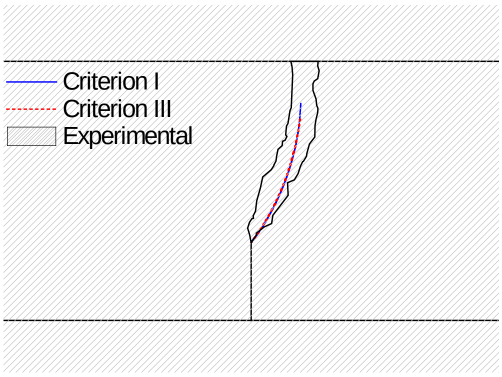

(j) FPS-80-20 Series

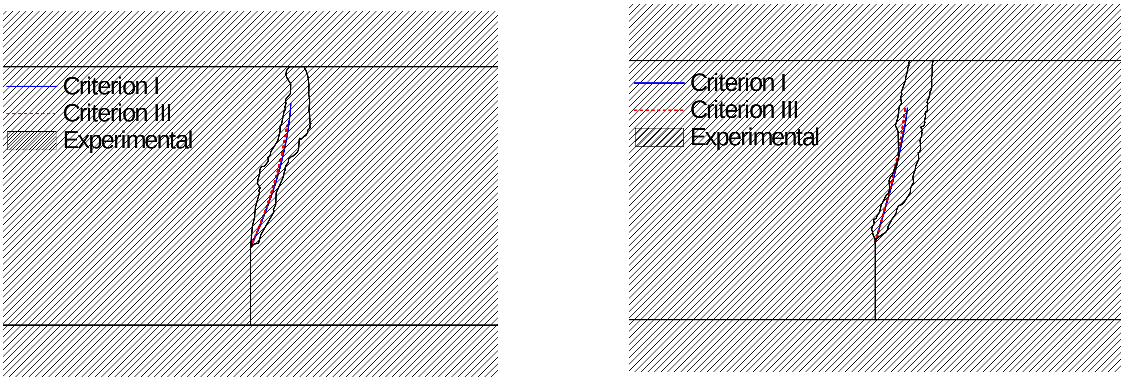

(k) FPS-80-40 Series (l) FPS-80-60 Series

Fig. 8. Crack trajectories from experiment and prediction using Criteria I and III

Effect of K_{II} on crack propagation

The difference between Criteria I and II falls on whether the components of K_{II}, including K_{II}^{P} and K_{II}^{σ}, are considered in the determination of crack propagation. Therefore, in this section, taking the concrete with C50 strength grade as an example, Fig. 9 illustrates the *P-CMS*D curves from numerical results using Criteria I and II. It should be noted that the specimens of FPS-50-0 series are almost solely mode II fracture corresponding to the crack initiation. It is unreasonable to determine the crack initiation for these specimens without considering the effect of K_{II}. Therefore, in the case of FPS-50-0 series, the crack initiation is determined using $K_{(\mathrm{I,\ II})}^{\mathrm{P}} - K_{(\mathrm{I,\ II})}^{\sigma} = K_{\mathrm{IC}}^{\mathrm{ini}}$ when both Criteria I and II are employed in the simulation. It can be seen from Fig. 9 that the predicted *P-CMSD* curves using Criteria I and II are almost identical and that the components of K_{II} in Criteria I and II have less effect on the predicted *P-CMSD* curves. However, the predicted initial fracture loads P_{ini} using the two criteria are obviously different. Table 6 lists P_{ini} obtained from experiment and predictions using Criteria I and II. Accordingly, a comparison is made between the predicted and experimental P_{ini} as shown in Fig. 10, in which $P_{\mathrm{ini,pre}}$ and $P_{\mathrm{ini,exp}}$ denote the predicted and experimental initial loads, respectively. It can be seen from this figure that, compared with the experimental results, the errors of predicted P_{ini} using Criterion II are larger than the ones using Criterion I, especially in the case of $K_{\text{I}}^{\text{ini}} / K_{\text{II}}^{\text{ini}}$=1.61. This is because the tip of the notched crack is under a mixed mode I-II stress field so the crack initiation should be dominated by the components of modes I and II SIFs. Fig. 11 illustrates the relationship of SIFs corresponding to crack initiation under three kinds of fracture modes, in which Points A, B and C denote the mixed mode I-II, mode I and mode II, respectively. For mode I and mode II fracture, the crack initiation is determined by the initial fracture toughness $K_{\text{IC}}^{\text{ini}}$ and $K_{\text{IIC}}^{\text{ini}}$, respectively. In the case of the mixed mode I-II fracture, the crack initiation is determined by the ratio of $K_{\text{I}}^{\text{ini}} / K_{\text{II}}^{\text{ini}}$, where $K_{\text{I}}^{\text{ini}}$ and $K_{\text{II}}^{\text{ini}}$ are the SIFs corresponding to crack initiation under mixed mode I-II fracture, so that $K_{\text{I}}^{\text{ini}} < K_{\text{IC}}^{\text{ini}}$ and $K_{\text{II}}^{\text{ini}} < K_{\text{IIC}}^{\text{ini}}$. If only using $K_{\text{IC}}^{\text{ini}}$, i.e. Criterion II, to determine the crack initiation under mixed mode I-II fracture, Point D, instead of Point A, denotes the crack initiation through increasing $K_{\text{I}}^{\text{ini}}$ to $K_{\text{IC}}^{\text{ini}}$. Obviously, the corresponding predicted P_{ini} will increase too, resulting in an overestimation of the initial cracking load. Particularly, the error will be larger with the decrease of the ratio of $K_{\text{I}}^{\text{ini}} / K_{\text{II}}^{\text{ini}}$. Therefore, the criterion including SIFs of modes I and II, i.e. Criterion I, is more appropriate for predicting the crack initiation of mixed mode I-II fracture.

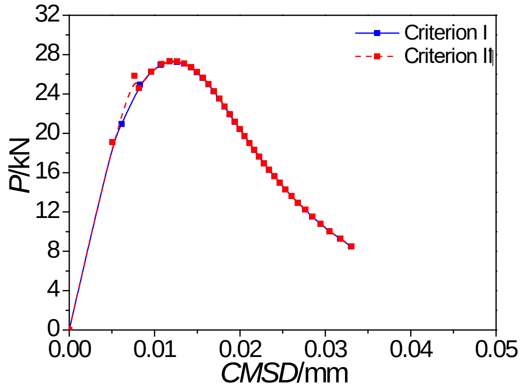

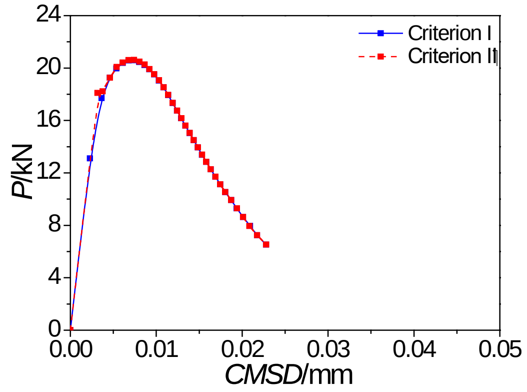

(a) FPS-50-0 Series

(b) FPS-50-20 Series

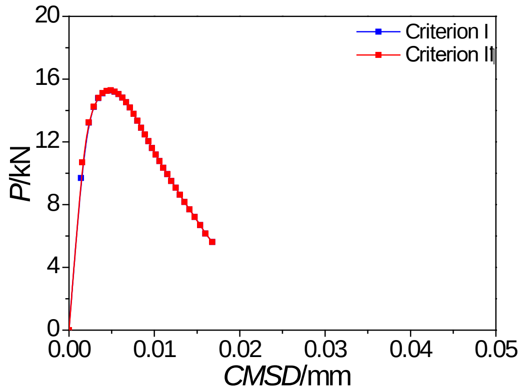

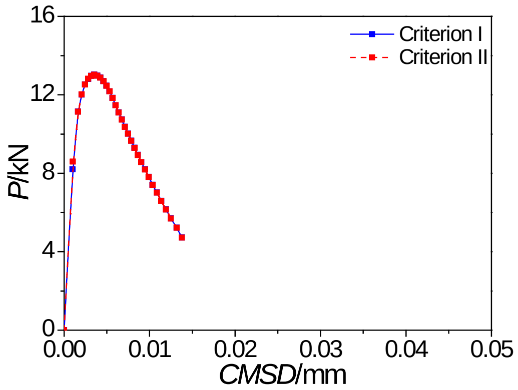

(c) FPS-50-40 Series

(d) FPS-50-60 Series

Fig. 9. *CMSD* curves from prediction using Criteria I and II

Table 6. Comparison of P_{ini} from experiment and prediction using Criteria I and II

Nos of specimens	Experimental (kN)	Criterion I (kN)	Error (%)	Criterion II (kN)	Error (%)
FPS-20-20	10.83	9.60	-11.35	13.20	21.88
FPS-20-40	7.16	7.10	-0.84	7.80	8.94
FPS-20-60	6.10	6.00	-1.64	6.20	1.64
FPS-50-20	13.77	13.10	-4.87	18.10	31.44
FPS-50-40	10.05	9.70	-3.48	10.70	6.47
FPS-50-60	7.67	8.20	6.91	8.60	12.12
FPS-80-20	12.40	13.90	10.79	19.20	48.92
FPS-80-40	10.89	10.30	-5.42	11.40	4.68
FPS-80-60	9.06	8.70	-3.97	9.10	0.44

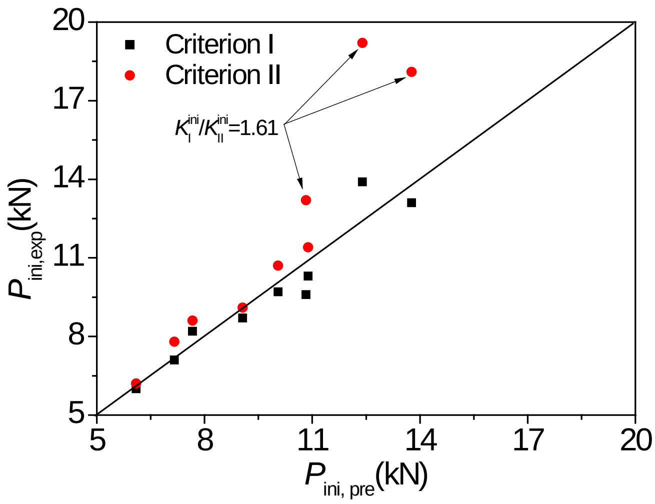

Fig. 10. P_{ini} obtained from experiment and prediction

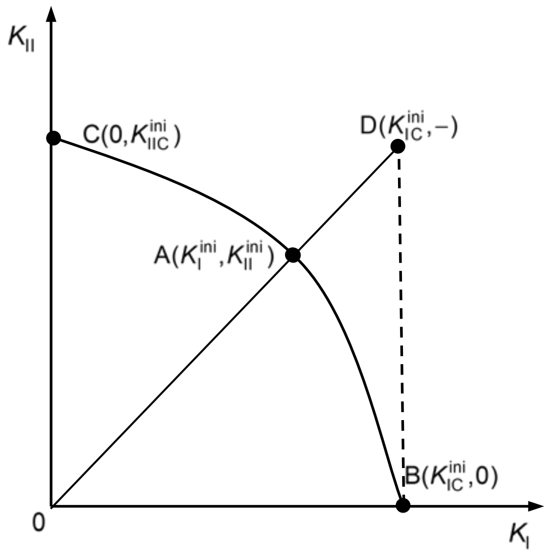

Fig. 11. Relationships of SIFs under different fracture modes

However, the ratio (i.e. K_{II}/K_I) will change after the crack initiation. Fig. 12 illustrates the variation of K_{II}/K_I during the crack propagation for FPS-50 series specimens. It can be seen that the ratio (i.e. K_{II}/K_I) decreases rapidly to approximately zero after crack initiation, which indicates that the fracture mode has transformed to mode I from mixed mode I-II. In this case, K_{II} has much less significant effect on the determination of crack propagation. Therefore, Criteria I and II are approximately equivalent in the determination of the crack propagation after crack initiation. It should be noted that the conclusion about the transformation of the fracture mode is based on the homogeneous assumption of concrete, i.e. the effects of aggregate bridging and crack deflection are not considered in this study.

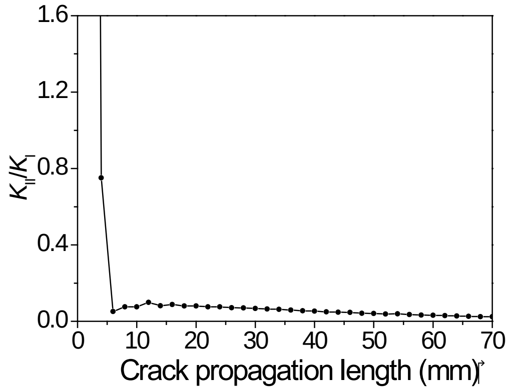

(a) FPS-50-0 Series

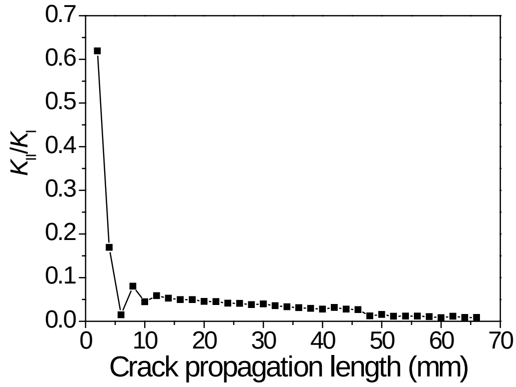

(b) FPS-50-20 Series

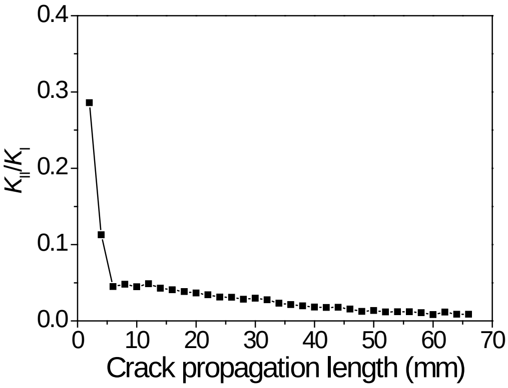

(c) FPS-50-40 Series

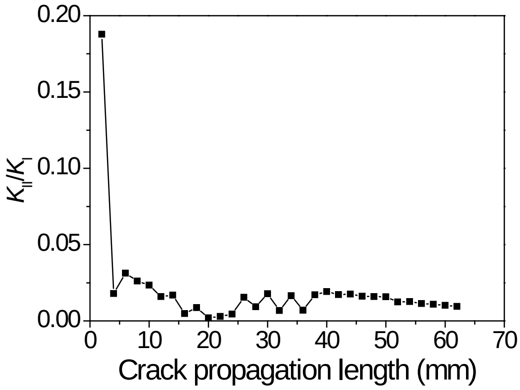

(d) FPS-50-60 Series

Fig. 12. Variation of K_{II}/K_I during the crack propagation

For Criteria III and IV, K_{IC}^{ini} is not considered as the crack propagation resistance. Thus, based on the two criteria, the crack will initiate under even a very small load and the fracture will transform into that of mode I dominated after that. Although the effect of K_{II} on the determination of crack propagation is introduced in Criterion III and not in Criterion IV, there is less significant effect of K_{II} on the crack propagation determination. Fig. 13 illustrates the P-CMSD curves of FPS-50 series of specimens from which it can be seen that the predicted curves using Criterion III are almost identical to the ones using Criterion IV.

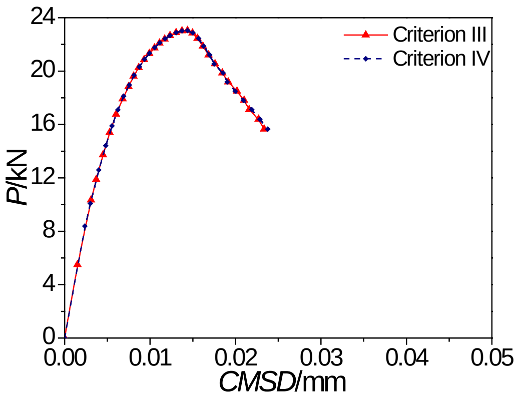

(a) FPS-50-0 Series

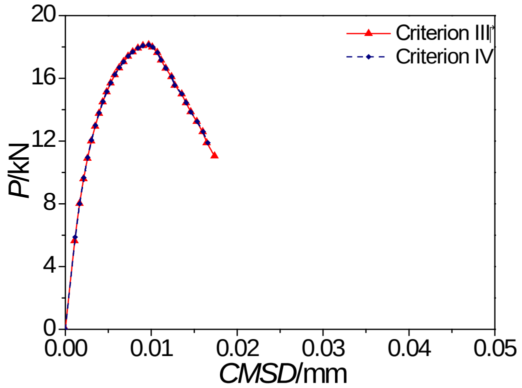

(b) FPS-50-20 Series

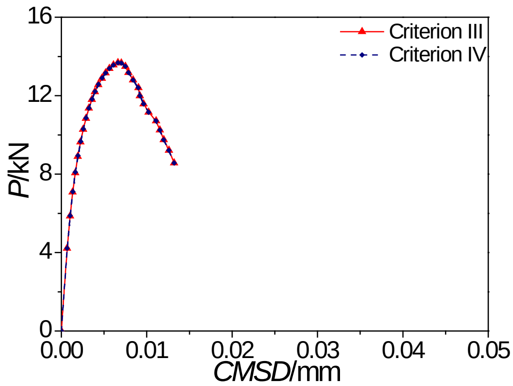

(c) FPS-50-40 Series

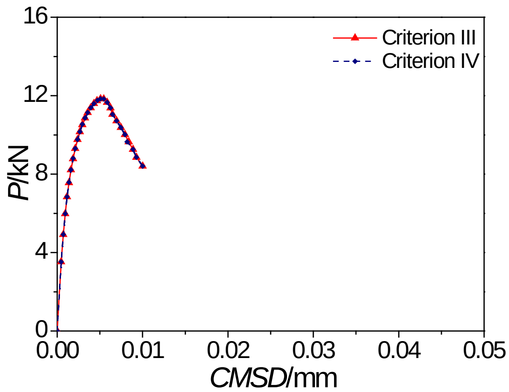

(d) FPS-50-60 Series

Fig. 13. Variation of K_{II}/K_{I} during the crack propagation

6. Conclusions

Four SIF-based criteria were used to determine the crack propagation of concrete under mixed mode I-II fracture and the whole fracture process was simulated based on the four criteria. A series of beams under four-point shear with different concrete strength grades were tested to measure *P-CMOD*, *P-CMSD* curves and crack propagation trajectory.

Compared with the experimental results, the predicted results by means of the four criteria showed different degrees of agreement. The effects of different criteria on the predicted results, including P_{ini}, P_{max}, *P-CMOD* and *P-CMSD* curves, were discussed. The following conclusions can be drawn:

(a) Compared with the experimental results, the predicted *P-CMOD* and *P-CMSD* curves using the initial fracture toughness-based criterion with K_{II} i.e. Criterion I, show a better agreement than the ones using the nil SIF-based criterion with K_{II}, i.e. Criterion III. With respect to Criterion III, the predicted P_{max} is smaller, but a_C, $CMOD_C$ and $CMSD_C$ are larger than the ones based on Criterion I. With the increase of the concrete strength, the errors of P_{max} between the experimental results and predictions using Criterion III approximately increase.

(b) K_{II} component in the criterion has a significant effect on the determination of the initial load of mixed mode I-II fracture. Compared with the experimental results, the predicted P_{ini} values are overestimated when the initial fracture toughness-based criterion without K_{II}, i.e. Criterion II, is employed. However, since the fracture transforms from the mixed mode I-II to mode I after the crack initiation, K_{II} component in the criterion has less effect on the crack propagation process. Therefore, the predicted *P-CMSD* curves using Criteria II almost coincided with the ones using Criterion I.

Among the four SIF-based criteria investigated in this study, the initial fracture toughness-based criterion with K_{II}, i.e. Criterion I, is more appropriate than the other three criteria in determining the crack propagation process of mixed mode I-II fracture.

Acknowledgement

The financial support of the National Natural Science Foundation of China under the grant of NSFC 51478084, NSFC 51421064, and partial finance support from the UK Royal Academy of Engineering through the Distinguished Visiting Fellow scheme under the grant DVF1617_5_21 is gratefully acknowledged.

References

[1] Hillerborg A, Modéer M, Petersson PE. Analysis of crack formation and crack growth in concrete by means of fracture mechanics and finite elements. Cem Concr Res. 1976;6:773-81.

[2] Shi Z. Numerical Analysis of Mixed-Mode Fracture in Concrete Using Extended Fictitious Crack Model. J Struct Eng. 2004;130:1738-47.

[3] Prasad MVKV, Krishnamoorthy CS. Computational model for discrete crack growth in plain and reinforced concrete. Comput Method Appl M. 2002;191:2699-725.

[4] Gálvez JC, Červenka J, Cendón DA, Saouma V. A discrete crack approach to normal/shear cracking of concrete. Cem Concr Res. 2002;32:1567-85.

[5] Cendón DA, Gálvez JC, Elices M, Planas J. Modelling the fracture of concrete under mixed loading. Int J Fracture. 2000;103:293-310.

[6] Kurumatani M, Terada K, Kato J, Kyoya T, Kashiyama K. An isotropic damage model based on fracture mechanics for concrete. Eng Fract Mech. 2016;155:49-66.

[7] Mirsayar MM, Razmi A, Berto F. Tangential strain-based criteria for mixed-mode I/II fracture toughness of cement concrete. Fatigue Fract Eng M. 2018;41:129-37.

[8] Mirsayar MM. Mixed mode fracture analysis using extended maximum tangential strain criterion. Mater Design. 2015;86:941-7.

[9] Menetrey P, Willam KJ. Triaxial failure criterion for concrete and its generalization. ACI Struct J. 1995;92:311-8.

[10] Yang ZJ, Proverbs D. A comparative study of numerical solutions to non-linear discrete crack modelling of concrete beams involving sharp snap-back. Eng Fract Mech. 2004;71:81-105.

[11] Yang Z, Chen J. Fully automatic modelling of cohesive discrete crack propagation in concrete beams using local arc-length methods. Int J Solids Struct. 2004;41:801-26.

[12] Malíková L. Multi-parameter fracture criteria for the estimation of crack propagation direction applied to a mixed-mode geometry. Eng Fract Mech. 2015;143:32-46.

[13] Bažant ZP, Li Y-N. Stability of Cohesive Crack Model: Part I—Energy Principles. Journal of Applied Mechanics. 1995;62:959-64.

[14] Carpinteri A, Massabó R. Reversal in Failure Scaling Transition of Fibrous Composites. J Eng Mech. 1997;123:107-14.

[15] Ooi ET, Yang ZJ. Modelling crack propagation in reinforced concrete using a hybrid finite element–scaled boundary

finite element method. Eng Fract Mech. 2011;78:252-73.
[16] Moës N, Belytschko T. Extended finite element method for cohesive crack growth. Eng Fract Mech. 2002;69:813-33.
[17] Yang ZJ, Deeks AJ. Fully-automatic modelling of cohesive crack growth using a finite element–scaled boundary finite element coupled method. Eng Fract Mech. 2007;74:2547-73.
[18] Ooi ET, Yang ZJ. A hybrid finite element-scaled boundary finite element method for crack propagation modelling. Comput Method Appl M. 2010;199:1178-92.
[19] Gálvez JC, Elices M, Guinea GV, Planas J. Mixed Mode Fracture of Concrete under Proportional and Nonproportional Loading. Int J Fracture. 1998;94:267-84.
[20] Zhong H, Ooi ET, Song C, Ding T, Lin G, Li H. Experimental and numerical study of the dependency of interface fracture in concrete–rock specimens on mode mixity. Eng Fract Mech. 2014;124-125:287-309.
[21] Foote RML, Mai Y-W, Cotterell B. Crack growth resistance curves in strain-softening materials. J Mech Phys Solids. 1986;34:593-607.
[22] Zhang J, Li VC. Simulation of crack propagation in fiber-reinforced concrete by fracture mechanics. Cem Concr Res. 2004;34:333-9.
[23] Mai Y-W. Cohesive zone and crack–resistance (R)-curve of cementitious materials and their fibre-reinforced composites. Eng Fract Mech. 2002;69:219-34.
[24] Dong W, Wu Z, Zhou X. Calculating crack extension resistance of concrete based on a new crack propagation criterion. Constr Build Mater. 2013;38:879-89.
[25] Wu Z, Wu X, Dong W, Zheng J, Wu Y. An analytical method for determining the crack extension resistance curve of concrete. Mag Concr Res. 2014;66:719-28.
[26] Dong W, Zhou X, Wu Z. On fracture process zone and crack extension resistance of concrete based on initial fracture toughness. Constr Build Mater. 2013;49:352-63.
[27] Qing LB, Tian WL, Wang J. Predicting unstable toughness of concrete based on initial toughness criterion. Journal of Zhejiang University-Science A. 2014;15:138-48.
[28] Wu Z, Rong H, Zheng J, Dong W. Numerical method for mixed mode I–II crack propagation in concrete. J Eng Mech, ASCE. 2013;139:1530-8.
[29] Dong W, Yang D, Zhang B, Wu Z. Rock-Concrete Interfacial Crack Propagation under Mixed Mode I-II Fracture. J Eng Mech. 2018;144:04018039.
[30] Petersson PE. Crack growth and development of fracture zones in plain concrete and similar materials. Division of Building Materials, Lund Institute of Technology, Report TVBM-1006, Sweden, 1981. 1981.
[31] Tada H, Paris PC, Irwin GR. The Stress Analysis of Cracks Handbook. New York, USA: ASME; 2000.
[32] Li C-Q, Fu G, Yang W, Yang S. Derivation of elastic fracture toughness for ductile metal pipes with circumferential external cracks under combined tension and bending. Eng Fract Mech. 2017;178:39-49.
[33] Shah SP. Size-effect method for determining fracture energy and process zone size of concrete. Mater Struct. 1990;23:461.
[34] Karamloo M, Mazloom M, Payganeh G. Effects of maximum aggregate size on fracture behaviors of self-compacting lightweight concrete. Constr Build Mater. 2016;123:508-15.
[35] Elices M, Rocco CG. Effect of aggregate size on the fracture and mechanical properties of a simple concrete. Eng Fract Mech. 2008;75:3839-51.
[36] Siregar APN, Rafiq MI, Mulheron M. Experimental investigation of the effects of aggregate size distribution on the fracture behaviour of high strength concrete. Constr Build Mater. 2017;150:252-9.
[37] Guan JF, Li QB, Wu ZM, Zhao SB, Dong W, Zhou SW. Fracture parameters of site-cast dam and sieved concrete. Mag Concr Res. 2016;68:43-54.
[38] Guan J, Hu X, Li Q. In-depth analysis of notched 3-p-b concrete fracture. Eng Fract Mech. 2016;165:57-71.

[39] Hu XZ, Duan K. Mechanism behind the size effect phenomenon. J Eng Mech-ASCE. 2010;136:60-8.
[40] Guan J, Hu X, Yao X, Wang Q, Li Q, Wu Z. Fracture of 0.1 and 2 m long mortar beams under three-point-bending. Mater Design. 2017;133:363-75.
[41] Hu XZ, Guan JF, Wang YS, Keating A, Yang ST. Comparison of boundary and size effect models based on new developments. Eng Fract Mech. 2017;175:146-67.
[42] Guan JF, Hu XZ, Xie CP, Li QB, Wu ZM. Wedge-splitting tests for tensile strength and fracture toughness of concrete. Theor Appl Fract Mec. 2018;93:263-75.

Nomenclature

a	crack length
a_0	initial crack length
a_C	critical crack length
B	width of three-point beam
$CMOD$	crack mouth opening displacement
$CMOD_C$	critical crack mouth opening displacement
$CMSD$	crack mouth sliding displacement
$CMSD_C$	critical crack mouth sliding displacement
D	height of three-point beam
E	elastic modulus
f_c	uniaxial compressive strength of concrete
f_t	splitting tensile strength of concrete
G_f	fracture energy
H_0	thickness of the knife edge
K_I	difference of SIFs of mode I caused by applied load and cohesive force
K_{II}	difference of SIFs of mode II caused by applied load and cohesive force
K_P	SIF caused by applied load
K_σ	SIF caused by cohesive force
K_m	critical fracture toughness of mortar
K_{IC}^{ini}	initial fracture toughness of concrete
K_I^P	SIFs of mode I caused by applied load
K_I^σ	SIFs of mode I caused by cohesive force
K_{II}^P	SIFs of mode II caused by applied load
K_{II}^σ	SIFs of mode II caused by cohesive force
L	length of three-point beam
P	applied load
P_{ini}	initial cracking load
$P_{ini,exp}$	measured initial load
$P_{ini,pre}$	predicted initial load from experiment
P_{max}	peak load
$P_{max,exp}$	measured peak load from experiment
$P_{max,pre}$	predicted peak load
α	crack propagation angle
Δa	crack propagation length
σ	cohesive stress
σ_s	stress corresponding to the break point in bilinear σ-w relationship
w	crack opening displacement
w_s	displacement corresponding to the break point in bilinear σ-w relationship
w_0	stress-free crack width